

BIG BANG NUCLEOSYNTHESIS DEEP UNDERGROUND

Carlo Gustavino
INFN-Roma
(for the LUNA collaboration)

Abstract

Big Bang Nucleosynthesis (BBN) theory provides definite predictions for the abundance of light elements produced in the early universe. At BBN energies ($30 \lesssim E_{cm} \lesssim 300$ MeV) the cross section of many BBN nuclear reactions is very low because of the Coulomb repulsion between the interacting nuclei. In order to reduce the cosmic ray induced background it is convenient to perform the measurements deep underground. In this presentation the BBN measurements of LUNA (Laboratory for Underground Nuclear Astrophysics) are reviewed. In particular, It will be shown that the ongoing study of the $D(p, \gamma)^3He$ reaction is of primary importance to derive the baryon density of universe Ω_b . Moreover, this study allows to constrain the existence of the so called "dark radiation", composed by undiscovered relativistic species permeating the universe, such as sterile neutrinos.

1 Introduction

The Big Bang nucleosynthesis (BBN) theory describes the formation of light nuclides during the first minutes of cosmic time, when the Universe was hot, dense and rapidly expanding. Assuming standard physics, the synthesis of light isotopes depends on the nuclear reactions shown in figure 1. The nucleosynthesis begins with the formation of deuterium by $p(n,\gamma)^2\text{H}$ reaction. Subsequently, ^3H and ^3He are produced via the $^2\text{H}(^2\text{H},p)^3\text{H}$, $^2\text{H}(^2\text{H},n)^3\text{He}$ and $^2\text{H}(p,\gamma)^3\text{He}$ processes. The $^3\text{H}(^2\text{H},n)^4\text{He}$ and $^3\text{He}(^2\text{H},p)^4\text{He}$ reactions produce ^4He , in which nearly all the free neutrons end up bound, while the abundances of deuterium, tritium and ^3He are relatively small (residual tritium is successively converted into ^3He via weak decay). The primordial abundance of heavier isotopes ^7Li and ^6Li is even smaller (after BBN, the produced ^7Be decays into ^7Li), because the absence of stable nuclei with mass number 5 impedes nucleosynthesis via $^4\text{He} + n$ and $^4\text{He} + p$ reactions. Finally, the production of nuclides with $A > 8$ is negligible, because the lack of stable nuclei with $A = 8$ prevents nuclear reactions through the $^4\text{He} + ^4\text{He}$ channel to occur.

In standard cosmology, the expansion rate of the universe is governed by the Friedmann equation:

$$H^2 = \frac{8\pi}{3}G\rho, \quad (1)$$

where H is the Hubble parameter, G is the Newton's gravitational constant and ρ is the energy density which, in the early Universe, is dominated by the "radiation", i.e. the contributions from massless or extremely relativistic particles. The only known relativistic particles at the BBN epoch are the photons and the three neutrino families. Therefore, the radiation density can be expressed as follows:

$$\rho = \rho_\gamma \left[1 + \frac{7}{8} \left(\frac{4}{11} \right)^{4/3} N_{eff} \right]. \quad (2)$$

In this formula ρ_γ is the photon density and N_{eff} is the contribution of other relativistic species. Using this formula $N_{eff} = 3.046$ if only the three known neutrino families are considered. Assuming standard physics, the only free parameter in the BBN theory is the baryon density Ω_b or equivalently η , defined as the ratio of baryons with respect to photons.

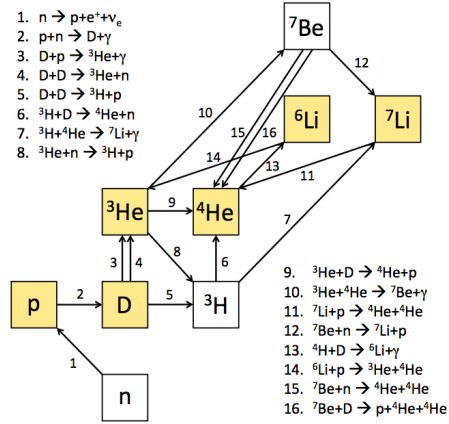


Figure 1: Leading processes of Big Bang Nucleosynthesis. Yellow boxes mark stable isotopes.

Figure 2 shows the calculated abundance of ${}^4\text{He}$, D and ${}^7\text{Li}$ as a function of η (the uncertainty is represented by the red, blue and orange bands, respectively). In this figure are also shown the results of astronomical observations (horizontal bands) and the η value derived from CMB data (vertical band) [1–5]. Table 1 summarises the results of BBN calculations (assuming the Λ CDM model and the η parameter derived from CMB experiments) and the results of direct observations. The computed ${}^4\text{He}$ abundance essentially depends on the amount of free neutrons available, therefore its (very small) uncertainty is almost entirely due to the neutron lifetime error [6]. The primitive abundance of ${}^4\text{He}$ derived from observations is deduced from observations in HII (ionized hydrogen) regions of compact blue galaxies. The uncertainty is mainly due to systematics such as plasma temperature or stellar absorption [2]. Apart from helium, the calculated abundances of all the other nuclides strongly depend on the details of the BBN reaction chain [6]. The abundance of deuterium has been recently derived with good accuracy from the observation of Damped Lyman-Alpha (DLA) systems at high redshift [4]. Note that the error of $(D/H)_{BBN}$ is larger than the $(D/H)_{obs}$ one, mainly because of the paucity of data of the deuterium burning reaction ${}^2\text{H}(p,\gamma){}^3\text{He}$ [7]. The $({}^3\text{He}/H)_{BBN}$ value has a quite small error, while the ${}^3\text{He}$ observations in our galaxy are affected by large systematical

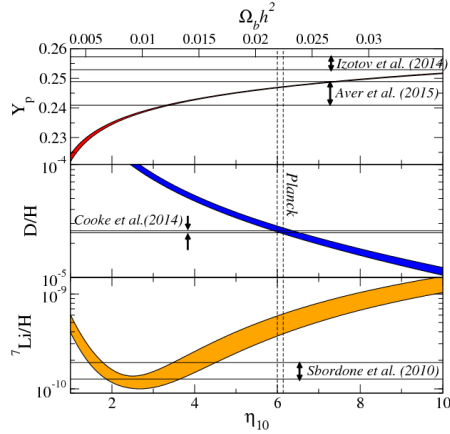


Figure 2: Abundance of light elements produced in standard BBN as a function of η (see text). The vertical region $\Omega_b h^2 = 0.02222 \pm 0.00023$ indicates the constraint from Planck.

uncertainties. In fact, this isotope is both produced and destroyed in stars so that its primordial amount is quite uncertain [8]. Therefore, up to now ^3He does not represent a powerful probe to constrain the ΛCDM model. The abundance of ^7Li is deduced from the strength of its characteristic absorption line at about 680 nm in low metallicity stars in the galactic halo. The observations show that the lithium abundance is almost independent of metallicity (“Spite plateau” [9]). This asymptotic value is interpreted as the primordial ^7Li abundance pointing out the tension between observations and theory, referred in literature as the “lithium problem”. Finally, a controversial measurement is reported in literature in which the ^6Li abundance is obtained from the analysis of metal poor stars absorption spectra [10]. Even though many of the claimed ^6Li detections are questionable, for a very few metal-poor stars there still seems to be a significant amount of ^6Li (“the second Lithium problem”) [11]. The theoretical ^6Li abundance has been recently well established by the LUNA collaboration with the first direct measurement of the cross section of the $^2\text{H}(^4\text{He}, \gamma)^6\text{Li}$ process at BBN energies.

Although primordial abundances span many orders of magnitude, observations and theory are fairly in agreement, thus confirming the overall validity of BBN

Table 1: Calculated and observed abundances of light isotopes derived from standard BBN and from direct astrophysical observations (see text). In this table, the primordial ${}^4\text{He}$ abundance is given in terms of the baryon mass fraction Y_p i.e. the ratio between helium and baryon densities. The abundance of the other nuclides is expressed by number ratios with respect ${}^1\text{H}$.

Isotope	SBBN Theory	Observations
Y_p	0.24771 ± 0.00014 [1]	0.254 ± 0.003 [2]
D/H	$(2.6 \pm 0.07) \times 10^{-5}$ [1]	$(2.53 \pm 0.04) \times 10^{-5}$ [4]
${}^3\text{He}/\text{H}$	$(1.00 \pm 0.01) \times 10^{-5}$ [14]	$(0.9 \pm 1.3) \times 10^{-5}$ [8]
${}^7\text{Li}/\text{H}$	$(4.68 \pm 0.67) \times 10^{-10}$ [14]	$(1.23^{+0.68}_{-0.32}) \times 10^{-10}$ [12]
${}^6\text{Li}/{}^7\text{Li}$	$(1.5 \pm 0.3) \times 10^{-5}$ [13]	$\lesssim 10^{-2}$ [10]

theory. However, some tension between theory and measurements is apparent, possibly due to the lack of knowledge of astrophysical processes or to physics beyond the Standard Model. As an example, the existence of extra relativistic species beside photons and standard neutrinos increases Y_p and (D/H) [4, 15], while the abundance of lithium isotopes can be affected by new physics, such as the existence of supersymmetric particles at the BBN epoch [16–19]. In this concern, BBN is a powerful tool to constrain particle physics and cosmology, with accuracy depending on astronomical observations and nuclear cross section measurements.

2 Underground Nuclear Astrophysics

BBN started when the temperature of the Universe was low enough to break the equilibrium between deuteron production through $p(n,\gamma){}^2\text{H}$ ($Q = 2.2 \text{ MeV}$) and its photo-dissociation through ${}^2\text{H}(\gamma,n)p$ (“deuterium bottleneck”). Consequently, BBN processes occur at relatively low energies ($30 \lesssim E_{cm}(\text{keV}) \lesssim 300$). In this energy range the cross-section $\sigma(E)$ drops almost exponentially with decreasing energy E , because of the coulomb barrier between the positively charged nuclei. For this reason the cross section is usually factorised as shown in the following formula [20]:

$$\sigma(E) = \frac{S(E)e^{-2\pi\eta^*}}{E} \quad (3)$$

Table 2: List of the leading reactions and corresponding rate symbols controlling the deuterium abundance after BBN. The last column shows the error on the ratio $(D/H)_{BBN}$ coming from experimental (or theoretical) uncertainties in the cross section of each reaction, for a fixed baryon density $\Omega_b h^2 = 0.02207$ [7].

Reaction	Rate Symbol	$\sigma_{D/H} \cdot 10^5$
$p(n, \gamma)^2H$	R_1	± 0.002
$d(p, \gamma)^3He$	R_2	± 0.062
$d(d, n)^3He$	R_3	± 0.020
$d(d, p)^3H$	R_4	± 0.0013

$S(E)$ is the astrophysical factor and contains all the nuclear effects. For non-resonant reactions, $S(E)$ is a smoothly varying function of energy. The exponential term takes into account the coulomb barrier. The Sommerfeld parameter η^* is given by $2\pi\eta^* = 31.29Z_1Z_2(\mu/E)^{1/2}$. Z_1 and Z_2 are the nuclear charges of the interacting nuclei, μ is their reduced mass (in units of a.m.u.), and E is the center of mass energy (in units of keV).

At the earth's surface, the low experimental reaction yield makes the measurements severely hampered by the cosmic ray induced background. On the other hand, the cross section extrapolation from high energy data can lead to substantial uncertainties, because the contribution of narrow or subthreshold resonances can partially or completely dominate the reaction rate. To overcome this problem the LUNA collaboration has carried out its measurements underground, at the "Laboratori Nazionali del Gran Sasso" (LNGS). Here, the mountain provides a natural shielding which reduces the muon and neutron fluxes by a factor 10^6 and 10^3 , respectively. The suppression of the cosmic ray induced background also allows an effective suppression of the γ ray activity by a factor $10^{-2} \div 10^{-5}$, depending on the γ energy.

3 The ${}^2H(p, \gamma){}^3He$ reaction and the primordial deuterium abundance

As shown in table 2, the 3% error of $(D/H)_{BBN}$ is mainly due to the poor knowledge of the ${}^2H(p, \gamma){}^3He$ S-factor (S_{12}) at BBN energies. The experimental data are reported in figure 3. In the relevant energy range only a single

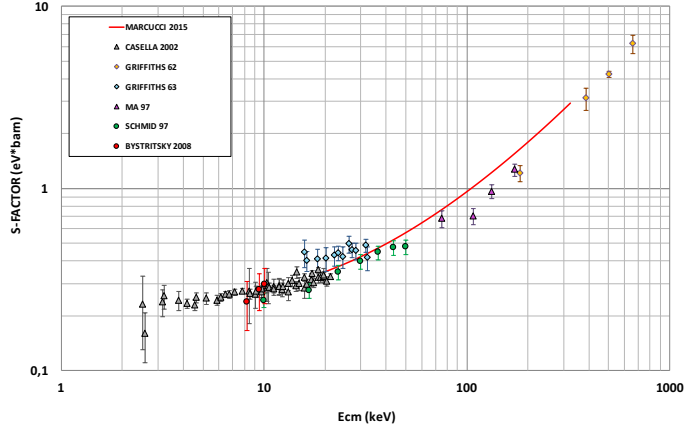


Figure 3: S-factor data for the reaction ${}^2\text{H}(p;\gamma){}^3\text{He}$. the red solid curve shows the prediction of recent ab initio theoretical calculation.

dataset of S_{12} is currently available in [21], in which the authors state a systematic error of 9%. The figure 3 also shows the behaviour of S_{12} as obtained by "ab initio" calculations [22]. The concern for ${}^2\text{H}(p,\gamma){}^3\text{He}$ error is made worse by the fact that the theoretical and experimental values of the S_{12} do not agree at the level of 20%. The existing difference between theory and data let some author to adopt the theoretical curve (see for example [15]) or the S_{12} value obtained from measurements [4, 23].

The LUNA collaboration measured the ${}^2\text{H}(p,\gamma){}^3\text{He}$ reaction in the Solar Gamow peak ($2.5\text{ keV} < E < 22\text{ keV}$) in 2002 [24], away from the BBN energy range ($30 \lesssim E_{cm}(\text{keV}) \lesssim 300$). However, the LUNA data definitely clarified the situation in the low energy range where previous experimental results differed by more than 50% [25]. Moreover, the inclusion of the new LUNA data increased the accuracy of the S-factor parametrization by a factor 3, when compared to previous analyses [26]. The abundance of deuterium strongly depends on the baryon density (see figure 2). The comparison of observed abundance with the value obtained with standard BBN theory and present literature data provides

the following value for the baryon density [4]:

$$\Omega_{b,0}(BBN) = (2.202 \pm 0.019 \pm 0.041)/h^2 \quad (4)$$

In this equation, $\Omega_{b,0}$ is the present day baryon density of universe and h is the Hubble constant in units of $100 \text{ km s}^{-1} \text{ Mpc}^{-1}$. The error terms in eq. (2) reflect the uncertainties in, respectively, observed deuterium abundance and BBN calculation [4]. Therefore, the baryon density accuracy is limited by the the poorly known $d(p, \gamma)^3\text{He}$ cross section. The baryon density is derived with similar accuracy from CMB experiments [1]:

$$\Omega_{b,0}(CMB) = (2.22 \pm 0.02)/h^2 \quad (5)$$

It is worth to point out that the baryon density derived from CMB data refers to the recombination epoch (about 380,000 years after Big Bang), while $\Omega_b(BBN)$ is the baryon density during the first minutes of Universe. Hence, the comparison of these two values represents a powerful probe to constrain the ΛCDM model. The deuterium abundance is also sensitive to the expansion rate of Uni-

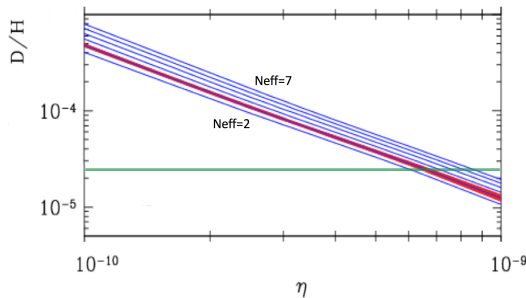


Figure 4: deuterium abundance as function of η . The blue lines indicate yields for a single value (integer plus 0.046) of N_{eff} . The red bands indicates the nuclear uncertainty for $N_{eff} = 3.046$. The horizontal green band indicates observational constraint on D abundance [4].

verse, that depends on the radiation density (see equations 1 and 2). Therefore, it allows to constrain the existence of extra relativistic particles besides photons and the three neutrino species (e.g. sterile neutrinos, hot axions, etc.). Figure 4 shows the calculated abundance of deuterium for several values of N_{eff} .

Again, more than the observed deuterium abundance $(D/H)_{obs}$, the sensitivity to "dark radiation" is limited by $(D/H)_{BBN}$ error, because of the ${}^2\text{H}(p,\gamma){}^3\text{He}$ cross section uncertainty.

A new study of the ${}^2\text{H}(p,\gamma){}^3\text{He}$ cross section is in progress at LUNA with the 400 kV accelerator [27], with the aim to measure the cross section of the ${}^2\text{H}(p,\gamma){}^3\text{He}$ reaction with an accuracy of $\lesssim 4\%$ and inside the BBN energy range ($30 < E_{cm} < 265$).

The experimental set up for the HPGe-phase consists of a 33 cm long windowless gas target (see figure 5). The target is high purity deuterium (99.9%) circulated at a pressure of 0.3 mbar in the target chamber. The target density has been accurately determined by measuring the pressure and temperature profile. The beam heating effect is of the order of 1% at the typical beam current (about 300 μA), and it has been measured by varying the current intensity from 30 to 400 μA .

A constant temperature gradient calorimeter serves as beam stopper and beam current measuring device. The beam impinges on the hot side of the calorimeter, which is heated up by thermoresistors to a constant temperature of 70 °C provided by a feedback controlled chiller. The cold side is cooled down to 0 °C. The difference between the heating power supply with and without beam is used to calculate the beam current.

Two Germanium detectors are implemented to detect the γ -rays radiating from inside the target chamber. The first detector (main detector, Ge1) is a 130% relative efficiency Germanium detector, faced to the middle of the gas chamber. The second detector (Ge2) has a 120% relative efficiency. It is movable along the beam axis and it is equipped with a lead collimator 50 mm thick, in such a way Ge2 mainly detects photons emitted in front of Ge2 and orthogonal to the beam line. To overcome the problem of measuring the Ge1 efficiency for photons with energy around 5.8 MeV (no source with sufficiently long life time produces photons close to this energy), it has been used a proton beam and a N_2 gas target at 4 mbar, to exploit the $E_R = 259$ keV resonance of the ${}^{14}\text{N}(p,\gamma_1\gamma_2){}^{15}\text{O}$ reaction. This reaction mainly produces two gamma in cascades with energy 5181+2375 keV (BR=17.1%), or 6172+1384 keV (BR=57.8%) or 6791+765 keV (BR=22.9%). In our working conditions the energy loss of proton beam in the gas target is about 1.32 keV/cm. Therefore, by properly tuning the proton beam energy, it is possible to face the

resonance position in front to the Ge2 detector, (see figure 5). In this way, the detection of the γ_1 photon with Ge1 (e.g. $E_{\gamma_1} = 1384 \text{ keV}$) acts as trigger for the coincident γ_2 photon ($E_{\gamma_2} = 6172 \text{ keV}$) eventually detected with Ge2. Figure 6 shows the Ge1 efficiency as a function of the position, for all the six energy of photons emitted by the $^{14}\text{N}(p, \gamma_1 \gamma_2)^{15}\text{O}$ reaction. The fine tuning of measured efficiency is obtained by means of a detailed MC simulation, to take into account of the angular correlation between the 2 gammas and to correct other second order effects.

The energy of photons emitted by the $^2\text{H}(p, \gamma)^3\text{He}$ reaction ($Q=5.5 \text{ MeV}$) is given by the following relationship (in which $c=\hbar=1$):

$$E_\gamma = \frac{m_p^2 + m_d^2 - m_{He}^2 + 2E_p m_d}{2(E_p + m_d - p_p \cos \theta)} \quad (6)$$

In this formula E_γ is the energy of emitted photon, m_p , m_d , m_{He} are the masses of proton, deuterium and ^3He , respectively. E_p and p_p are the energy and momentum of projectile, and θ is the angle of emitted photon in the laboratory system. This formula shows that the energy of a photon depends on its angle with respect of the beam direction (Doppler effect). Therefore, for a given proton energy, the full detected photons generate a slightly broad peak in the Ge1 energy spectrum, whose shape depends on the angular distribution of emitted photons (see figure 7). The data analysis is presently in progress. Hopefully, the new data will substantially improve the present baryon density determination and will allow to better constrain the existence of "dark radiation". Moreover, the measurement of total and differential cross section represents a solid reference to test theoretical "few body" calculations.

4 The $^3\text{He}(^2\text{H}, p)^4\text{He}$ reaction and the primordial ^3He abundance

The ^3He primordial abundance is mainly determined by the $^3\text{He}(^2\text{H}, p)^4\text{He}$ process and, to a lower extent, by the $\text{D}(p, \gamma)^3\text{He}$ reaction. Both reactions were studied at LUNA but outside the energy region of interest for BBN. Differently from the $^2\text{H}(p, \gamma)^3\text{He}$ case, the LUNA [28, 29] data for the $^3\text{He}(^2\text{H}, p)^4\text{He}$ reaction did not considerably increase the precision of the ^3He primordial abundance estimation. Moreover, it is very difficult to measure the ^3He primordial abundance from the astronomical point of view given that this isotope is created and destroyed during the stellar/galactic evolution. This explains why

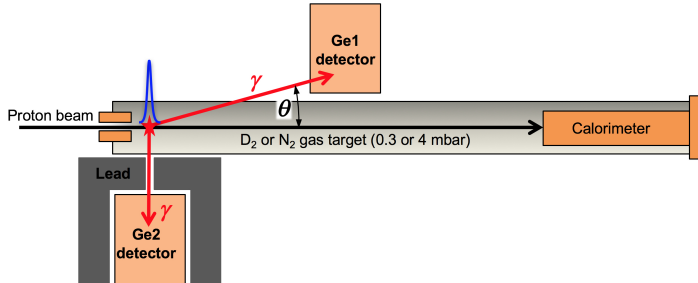


Figure 5: Drawing of the setup used to study the ${}^2\text{H}(p, \gamma){}^3\text{He}$ reaction. The efficiency of Ge1 is measured along the beam axes by exploiting the resonant reaction ${}^{14}\text{N}(p, \gamma_1 \gamma_2){}^{15}\text{O}$ (see text).

${}^3\text{He}$ was never used in the past as a cosmological baryometer due to the huge uncertainty on its observed value.

5 The ${}^3\text{He}(\alpha, \gamma){}^7\text{Be}$ reaction and the primordial ${}^7\text{Li}$ abundance

The BBN production of ${}^7\text{Li}$ is dominated by the ${}^3\text{He}(\alpha, \gamma){}^7\text{Be}$ reaction, with subsequent decay of radioactive ${}^7\text{Be}$ to ${}^7\text{Li}$. The ${}^3\text{H}(\alpha, \gamma){}^7\text{Li}$ reaction, on the other hand, plays only a minor role in ${}^7\text{Li}$ production [6]. The ${}^3\text{He}(\alpha, \gamma){}^7\text{Be}$ reaction was studied at LUNA using two different experimental techniques: First, with the detection of prompt emitted γ s by means of a large Ge(Li) detector faced to a windowless target chamber, in which the pressure of ${}^3\text{He}$ is maintained stable by a differential and recirculating pumping system. Second, the cross section was deduced from the ${}^7\text{Be}$ activity created in the experiment. Both methods took great advantage of the low radioactivity level of the underground Gran Sasso laboratory [30–32]. For three runs at different beam energies, both methods were used in parallel, allowing to check for possible systematic discrepancies between them. Just such a systematic discrepancy between activation and in-beam γ method had previously been suggested, giving rise to some uncertainty [33]. The LUNA data are shown figure 8), together with the results of other experiments. Note that the LUNA data are lower in energy than ever before and well inside the BBN energy region, with an accuracy of about 4%.

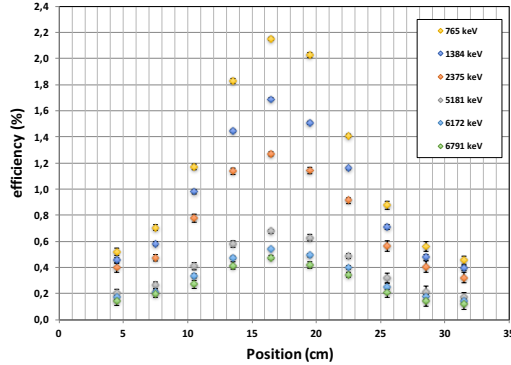


Figure 6: Efficiency of Ge1 detector as a function of the position along the beam line of the emitted photon, for several γ energies (see text).

6 The ${}^2\text{H}(\alpha,\gamma){}^6\text{Li}$ reaction and the primordial ${}^6\text{Li}$ abundance

If even one of the disputed ${}^6\text{Li}/{}^7\text{Li}$ detections, e.g. the one for HD 84937 [39–41], is confirmed, there remains the problem on how to produce ${}^6\text{Li}$ in very primitive stars without at the same time destroying all ${}^7\text{Li}$. Contrary to the case of ${}^7\text{Li}$ (see previous section), there are no standard physics solutions proposed for the production of ${}^6\text{Li}$. Standard BBN results in ${}^6\text{Li}/{}^7\text{Li} = (2\pm 3)\cdot 10^{-5}$ [6], much below the detected levels. As possible solution, it has been suggested a catalysis process by long-living particles and non-equilibrium BBN [16–18].

Standard BBN production of ${}^6\text{Li}$ is dominated by just one nuclear reaction, ${}^2\text{H}(\alpha,\gamma){}^6\text{Li}$ ($Q = 1.474\text{ MeV}$) [6]. Before LUNA, only direct measurements far away the BBN energy region were performed [36, 37] and, more recently, an indirect Coulomb dissociation experiments has been done [38]. Finally, for the first time, The ${}^2\text{H}(\alpha,\gamma){}^6\text{Li}$ cross section was directly measured at BBN energies by LUNA, strongly reducing the error due to extrapolations or theoretical assumptions. The setup used for the LUNA measurement is very similar to the one shown in figure shown in figure 5, but with only the Ge1 detector and an α beam instead of the proton one. The main problem encountered was the very small cross section (about 60 pbarn at $E = 133\text{ keV}$) and the relatively high beam induced background, much higher with respect to the environmental

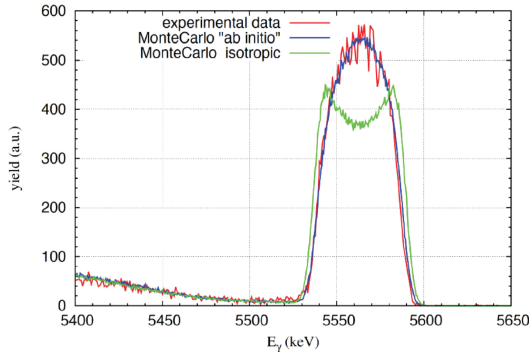


Figure 7: Simulated spectra of the ${}^2\text{H}(p, \gamma){}^3\text{He}$ reaction, assuming isotropic (green) and ab initio (blue) angular distribution at $E_{beam} = 167$ keV. The experimental data (red) are also shown. Data have been normalised to remark the close agreement with the ab initio angular distribution.

one but still more than one order of magnitude lower with respect the earth's surface one. The beam induced background is essentially due to deuterons scattered by the incident α beam that interact with other deuterons via the ${}^2\text{H}({}^2\text{H}, n){}^3\text{He}$ reaction, creating a low (about 10 s^{-1}) but steady neutron flux. The neutrons interact with the detector as well as with the setup materials, creating a beam induced background which exceeds the ${}^2\text{H}(\alpha, \gamma){}^6\text{Li}$ γ signal in the region of interest ($1590\text{ keV} < E_\gamma < 1625\text{ keV}$ at $E_\alpha = 400\text{ keV}$) by a factor of more than ten. Hence, a method to subtract the beam induced background has been developed [35].

7 Conclusion

Big Bang Nucleosynthesis is the natural connection between nuclear physics, cosmology and particle physics. The challenge for the next years is the improvement of astronomical observations of D , ${}^3\text{He}$, ${}^6\text{Li}$, ${}^7\text{Li}$ and the measurement of BBN cross section with very high accuracy, in order to shed light in many open problems in astrophysics, cosmology, particle physics. In this concern, underground nuclear astrophysics represents a major tool in the "precision era" of cosmology.

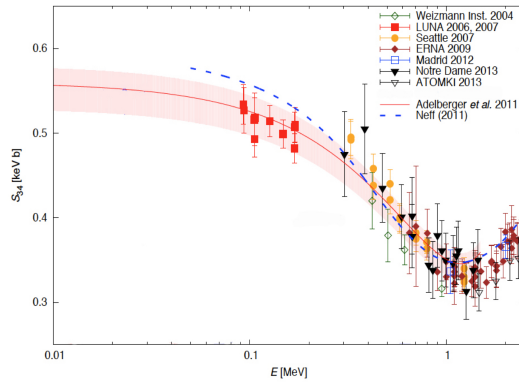


Figure 8: Astrophysical S-factor of the ${}^3\text{He}(\alpha,\gamma){}^7\text{Be}$ reaction. A theoretical curve rescaled to match the modern data [25], and ab-initio theory [34] are given.

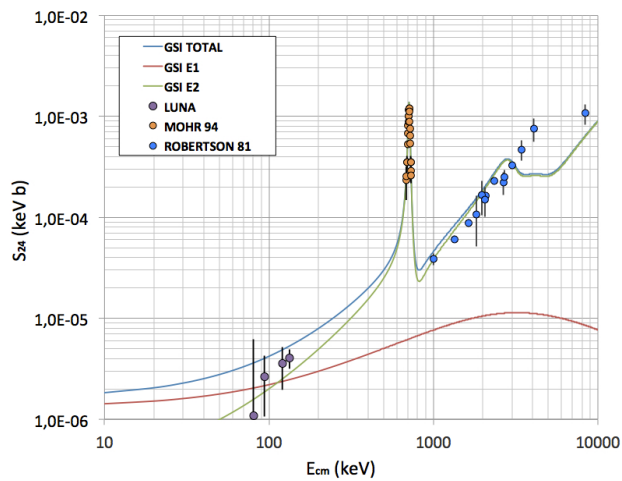


Figure 9: Astrophysical S-factor data of the ${}^2\text{H}(\alpha,\gamma){}^6\text{Li}$ reaction as a function of the center-of-mass energy. The LUNA data are shown with all the previous direct measurements [35–37]. The continuous lines show the theoretical E1, E2, and total S_{24} factors describing recent Coulomb dissociation data [38].

References

- 1 . Planck collaboration: AA **594**, A13 (2016)
- 2 . Y. I. Izotov et al., Astronomy & Astrophysics **558**, (2013) A57.
- 3 . E. Aver et al., JCAP **1311** (2013) 017.
- 4 . R. Cooke et al., Astrophys. J. **781** (2014) 31.
- 5 . L. Sbordone et al., Astron. Astrophys. **522** (2010) A26
- 6 . P. D. Serpico et al., Journ. of Cosm. and Astrop. Phys. **12**, (2004) 010
- 7 . E. Di Valentino et al., Physical Review D **90**, (2014) 023543
- 8 . T. Bania et al., Nature **415**, (2002) 54
- 9 . M. Spite and F. Spite, Nature **297**, (1982) 483
- 10 . M. Asplund et al., The Astrophysical Journal **644**, (2006) 229
- 11 . B. D. Fields, Ann.Rev. of Nucl. and Part. Science **61**, (2011) 47
- 12 . S. G. Ryan et al., The Astrophysical Journal Letters **530**, (2000) L57
- 13 . M. Anders et al, Physical Review Letters **113**, (2014) 042501
- 14 . R. H. Cyburt et al., Rev. Mod. Phys. **88**, (2016) 015004.
- 15 . K. M. Nollett and G. P. Holder, (2011) arXiv:1112.2683v1
- 16 . K. Jedamzik and M. Pospelov, New Journ. of Phys. **11** (2009) 105028 (2009)
- 17 . H. Djapo et al., Physical Review C **85**, (2012) 044602.
- 18 . M. Pospelov and J. Pradler, Ann. Rev. of Nucl. and Part. Science **60**, (2010) 539
- 19 . M. Kusakabe et al., Physical Review D **76**, (2007) 121302

- 20 . C. E. Rolfs, W.S.Rodney, "Cauldrons in the Cosmos", University of Chicago Press, Chicago,1988.
- 21 . L. Ma et al., Physical Review C **55**, (1997) 588
- 22 . L. E. Marcucci et al., PRL **116**, 102501 (2016)
- 23 . PLANCK collaboration: AA **571**, A16 (2014)
- 24 . C. Casella et al., Nuclear Physics A **706**, (2002) 203
- 25 . E. G. Adelberger et al., Review of Modern Physics **83**, (2011) 195
- 26 . R. H. Cyburt, Physical Review D **70**, (2004) 023505
- 27 . A. Formicola et al: Nucl. Inst. Meth. A **507**, (2003) 609
- 28 . H. Costantini et al., Physical Letters B **482**, (2000) 43
- 29 . M. Aliotta et al., Nuclear Physics A **690**, (2001) 790
- 30 . D. Bemmerer et al., Physical Review Letters **97**, (2006) 122502
- 31 . Gy. Gyürki et al., Physical Review C **75**, (2007) 035805
- 32 . F. Confortola et al., Physical Review C **75**, (2007) 065803
- 33 . E. Adelberger et al., Review of Modern Physics **70**, (1998) 1265
- 34 . T. Neff, Physical Review Letters **106**, (2011) 042502
- 35 . D. Trezzi et al., Astroparticle Physics **89** (2017) 57–65
- 36 . R. G. H. Robertson et al., Physical Review Letters **47**, (1981) 1867
- 37 . P. Mohr et al., Physical Review C **50**, (1994) 1543
- 38 . F. Hammache et al., Physical Review C **82**, (2010) 065803
- 39 . V. V. Smith et al., Astrophysical Journal **408**, (1993) 262
- 40 . R. Cayrel et al., Astronomy & Astrophysics **343**, (1999) 923
- 41 . M. Steffen et al., Memorie Societa Astronomica Italiana **22**, (2012) 152